

Purdue University

Purdue e-Pubs

---

International Refrigeration and Air Conditioning  
Conference

School of Mechanical Engineering

---

2022

## A White-box Modelling Methodology for Electronic Expansion Valve by Considering Choked Flow

Zhequan Jin

Noma Park

Byeong Hwi Lee

Yoonjei Hwang

Sim Won Chin

*See next page for additional authors*

Follow this and additional works at: <https://docs.lib.purdue.edu/iracc>

---

Jin, Zhequan; Park, Noma; Lee, Byeong Hwi; Hwang, Yoonjei; Chin, Sim Won; and Oh, Saikee, "A White-box Modelling Methodology for Electronic Expansion Valve by Considering Choked Flow" (2022). *International Refrigeration and Air Conditioning Conference*. Paper 2416.  
<https://docs.lib.purdue.edu/iracc/2416>

This document has been made available through Purdue e-Pubs, a service of the Purdue University Libraries. Please contact [epubs@purdue.edu](mailto:epubs@purdue.edu) for additional information. Complete proceedings may be acquired in print and on CD-ROM directly from the Ray W. Herrick Laboratories at <https://engineering.purdue.edu/Herrick/Events/orderlit.html>

---

**Authors**

Zhequan Jin, Noma Park, Byeong Hwi Lee, Yoonjei Hwang, Sim Won Chin, and Saikee Oh

# A White-box Modelling Methodology for Electronic Expansion Valve by Considering Choked Flow

Zhequan JIN<sup>1</sup>, Noma PARK<sup>1\*</sup>, Byeong Hwi LEE<sup>2</sup>, Yoonjei HWANG<sup>1</sup>,  
Sim Won CHIN<sup>2</sup>, Saikee OH<sup>1</sup>

<sup>1</sup>H&A R&D Center, Home Appliance & Air Solution Company, LG Electronics,  
51 Gasan Digital 1-Ro, Geumcheon Gu, Seoul, 08592, Republic of Korea  
Contact Information (+82-10-5625-6358, zhequan.jin@lge.com)

<sup>2</sup>Air Solution R&D Lab, Air Solution Business, Home Appliance & Air Solution Company, LG  
Electronics

84, Wanam-ro, Seongsan-gu, Changwon-si, Gyeongsangnam-do, 51554. Republic of Korea

\* Corresponding Author

## ABSTRACT

This work numerically investigates refrigerant expansion process through an EEV. Due to the multi-phase flow and complicated geometry inside, it is difficult to build a physical model to predict the refrigerant mass flow rate. Therefore, Bernoulli equation based polynomial or power-law fit correlation method and machine learning method (Grey-box Model) are applied to develop empirical EEV models so far. However, in this work, choked flow phenomenon is considered for proposing EEV's mass flow rate mapping method in the whole operating range. Theories of the flashing inception and the evaporation wave through the converging-diverging nozzles are involved. Moreover, momentum equation is calculated with finite volume method for metastable refrigerant converging flow. The developed novel method for EEV model is verified with laboratory based EEV's field performance data, showing the accuracy is within  $\pm 10\%$ .

## 1. INTRODUCTION

In the latest vapor compression air-conditioning systems, electronic expansion valve (EEV) is the most common refrigerant expansion device due to the advantage of fast system control with high precision. This is why the global EEV market size is expected to gain growth with a Compound Annual Growth Rate of 9.2% in the forecast period of 2020 to 2025 according to Fier Markets' report (2020).

As one of the most important control devices in vapor compression systems, the EEV model is critical not only for optimizing system control algorithm, but also for enabling automated fault detection and diagnostics. However, due to the multi-phase expansion process and complicated geometry inside of an EEV, it is difficult to build a physical model to predict refrigerant flow characteristics. Therefore, Eq. (1) based polynomial or power-law fitted mass flow coefficient ( $C_m$ ) correlation method or Artificial Neural Network (ANN) machine learning method is usually applied to develop empirical EEV models from experimental data.

$$\dot{m}_{eev} = C_m A_{eff} \sqrt{2\rho_L(P_{cond} - P_{eva})} \quad (1)$$

In fact, Eq. (1), derived from Bernoulli equation, was first developed by Wile (1935) for expansion valve investigation. Afterwards, the power-law fitted correlation method is widely used for EEV mass flow correlation (Zhang et al., 2006; Park et al., 2007; Xue et al., 2008; Chen et al., 2009). Moreover, Artificial Neural Network (ANN) machine learning method (Tian et al., 2015; Cao et al., 2016; Wan et al, 2020) also adopted the form of Eq. (1) to show the dimensionless output as shown by following Eq. (2).

$$y = \frac{\dot{m}_{eev}}{D_{eff}^2 \sqrt{\rho_L(P_{cond} - P_{eva})}} \quad (2)$$

However, Eq. (1) has obvious limitation to model two-phase mass flow characteristics because partial vaporization may take place at downstream of expansion process. Therefore, Roming et al. (1966), Davies and Daniels (1973), Li (2013), and Knabben et al. (2020) all introduced expansion factor  $Y$  and refined the Eq. (1) to Eq. (3) to deal with two-phase situations more accurately. In fact, the expansion factor  $Y$  accounts for the change in density as

the fluid passes from the valve inlet to the vena contracta and the change in area of vena contracta as pressure differential varied.

$$\dot{m}_{eev} = C_m A_{eff} Y \sqrt{2\rho_L (P_{cond} - P_{eva})} \quad (3)$$

From thermodynamics and fluid flow point of view, all of 3 equations listed above can be considered as highly simplified Grey-box models, which need part of physiological knowledge and part of refined datasets. This is due to the determination of  $C_m$  or  $Y$  value must rely on thousands of data from experiment or CFD results to ensure the EEV model's accuracy. In this way, thermodynamic specialist have to invest much extra labor to collect data for different EEV products and refrigerant before its engineering application.

Therefore, White-box EEV modelling methodology is necessary to be developed, which can reduce the engineering work load by focusing on full physiological knowledge of refrigerant's expansion process. However, the rapid depressurization inside of EEV makes thermodynamic behaviors quite complex, even the choked flow phenomenon happens when the pressure difference is big enough along with low subcooled degree.

In order to quantitatively investigate refrigerant's choked flow characteristics through EEV, Liu et al., (2008) calculated choking mass flow rate and maximal choking occurrence pressure by combining metastable liquid's flashing inception correlation and evaporation wave theory. Abuaf et al., (1983) presented a unified theory of inception criteria for critical flashing flows with subcooled inlets. They proposed a general correlation for pressure undershoot at flashing inception, which considered the effect of turbulence intensity in converging flows and convective depressurization rate based on previous work of Jones (1979) and Alamgir & Lienhard (1979). The verification of flashing inception correlation gives accurate prediction of the pressure undershoot at inception and the critical mass flow rates in nozzles. In addition, Simoes-Moreira et al., (2000, 2002, 2003) investigated the maximal choking occurrence pressure by adopting evaporation wave theory. In fact, evaporation wave is a discontinuity process, which need to be analyzed by the conservations of mass, momentum, and energy for a control volume enveloping the evaporation front. However, the choked flow mass flow rate was calculated by Bernoulli equation, Eq. (1), with empirical mass flow coefficient value of  $0.94 \pm 0.04$ , since the refrigerant between the entrance and the throat is assumed as single liquid.

This work, standing on the shoulders of above research work, aims to propose a EEV's mass flow rate mapping method by introducing a choked and non-choked mass flow rate profile. The well-studied theory of flashing inception and evaporation wave are involved for the calculation of profile's choked flow criteria. Moreover, the highlight is usage of momentum equation instead of Bernoulli equation for mass flow rate calculation in the converging flow section, and the momentum equation is numerically calculated with finite volume method. With this method, the EEV mass flow rate map of the whole engineering operation range of vapor compression air-conditioning systems can be easily generated by varying upstream refrigerant conditions and EEV openness.

## 2. MODELING METHODOLOGY

Fig.1 shows the EEV's choked and non-choked mass flow rate profile, from which it can be observed that non-choked mass flow rate increases with lower downstream pressure and choked mass flow rate remains constant. Therefore, in this section different EEV modeling methodology will be introduced to choked flow and non-choked flow conditions.

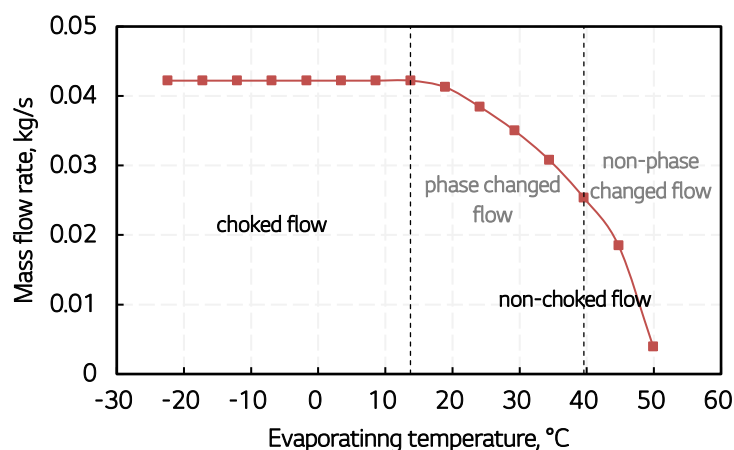


**Figure 1:** EEV's choked and non-choked mass flow rate profile

Fig.2 shows geometry and components inside of a typical EEV. In the scope of this study, EEV's complex 3-D geometry is simplified to 1-D variable area capillary analogy for the purpose of theoretical analysis. In addition, following assumptions are necessary to simplify problems for different models in the expansion process.

- Expansion process is assumed to be adiabatic;
- Flashing inception point is located at the throat;
- Flashing process is regarded as evaporation wave;
- Refrigerant immediately downstream the evaporation wave is in homogenous and thermal equilibrium.

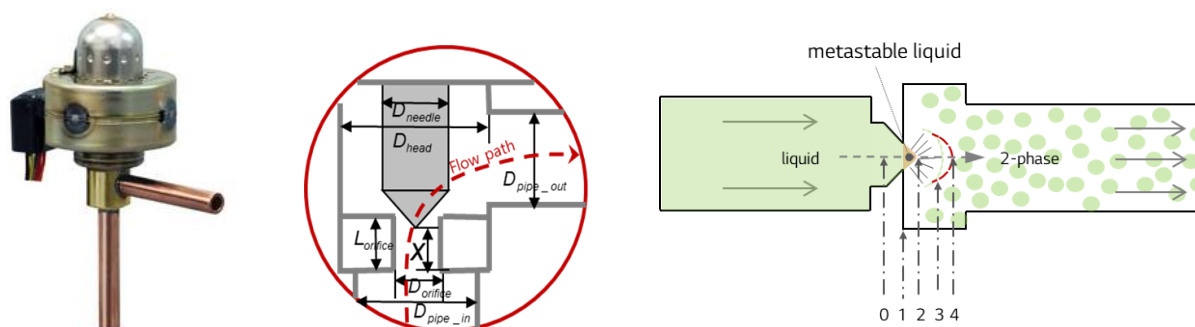


**Figure 2:** Geometry and refrigerant expansion process inside of EEV

## 2.1 Choked flow condition

The most important calculation criteria for choked flow condition is the choking mass flow rate and maximal choking occurrence pressure. As illustrated from P-log v diagram in Fig.3, in choked flow process, subcooled refrigerant (0) firstly depressurizes below to saturation pressure  $P_s$  of the inlet temperature at converging section of EEV. This results in a metastable liquid state of refrigerant (0→1) and make flashing inception occurs close to the throat (1) of EEV. Afterwards, explosive evaporation phenomenon, taking the shape of a cone (2), happens at exit of converging section of EEV undergoing a sudden phase transition (1→2), which is called evaporation wave. If EEV exit pressure is lower than the maximal choking occurrence pressure, this two-phase refrigerant flow continues expanding to supersonic (2→3). Afterwards, the supersonic flow undergoes a shock wave (3→4) accompanied with an abrupt pressure rise to match the EEV exit pressure. However, the shock wave will approach to the evaporation wave with increment of the EEV exit pressure, and it will disappear if the EEV exit pressure is equal to the maximal choking occurrence pressure. At this condition, one can calculate the choking mass flow rate and maximal choking occurrence pressure, because the upstream of shock wave is just overlapped with downstream of the evaporation wave and the velocity is sonic.

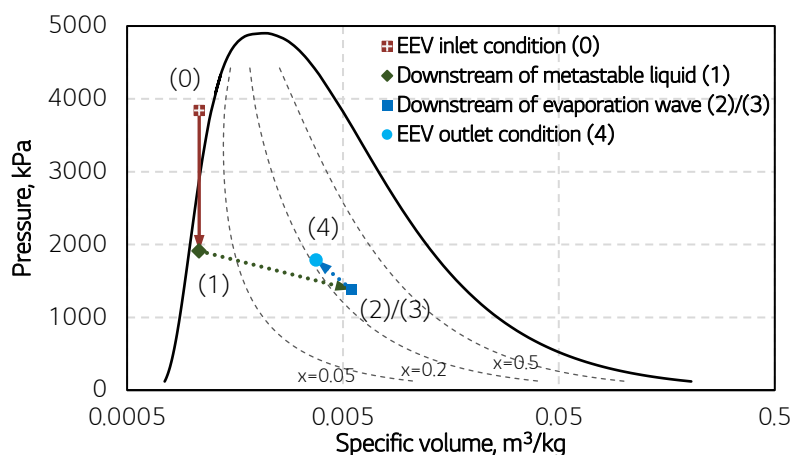


**Figure 3:** R410A expansion stages under choked flow condition in P-log v diagram

### Stage (0→1)

Abuaf et al., (1983) updated the dimensionless pressure undershoot at flashing inception by considering the effect of turbulence intensity in converging flows instead of straight pipes flow. Their model yielded following dimensionless pressure undershoot at flashing inception  $\Delta P_{Fi}^*$  from subcooled inlet conditions to metastable state.

$$\Delta P_{Fi}^* = \frac{\Delta P_{Fi}}{\Delta P_{Fio}} = \text{Max} \left\{ 0, 1 - 27 \left[ \frac{\overline{u}^2}{u_i^2} \right] \left[ \frac{A_{Fi}}{A_{in}} \right]^n Fi \right\} \quad (4)$$

where  $\Delta P_{Fi}$  is the flashing inception pressure undershoot

$$\Delta P_{Fi} = P_s - P_{Fi} \quad (4-1)$$

$\Delta P_{Fio}$  is the static flashing inception pressure undershoot, which is based on Alamgir & Lienhard;s (1979) semi-empirical model

$$\Delta P_{Fio} = 0.253 \frac{\sigma^{1.5} T_r^{13.73} \sqrt{1 + 14\Sigma^{0.8}}}{\sqrt{kT_c} \left(1 - \frac{v_L}{v_V}\right)} \quad (4-2)$$

here  $\Sigma$  is the decompression rate, which only considers the convective decompression rate due to steady flow

$$\Sigma = \frac{G_{choke}^3 d[\ln(A)]}{\rho_L^2 dz} \quad (4-2-1)$$

Since the turbulence effects is small in many converging flows, the value of turbulent intensity  $\frac{\sqrt{\overline{u}^2}}{u_i}$  can be set to 0.072, which is reasonable for the fully developed flow in a straight pipe preceding the nozzle according to Jones' (1979) work.

$Fi$  is flashing index, which is the inverse value of cavitation index

$$Fi = \frac{\rho_L u^2}{2\Delta P_{Fio}} \quad (4-3)$$

At last, the exponent index in Eq. 4 is defined as follows

$$n = \begin{cases} 1.75, & \frac{A_{Fi}}{A_{in}} \geq 1/6 \\ 1.4, & \frac{A_{Fi}}{A_{in}} < 1/6 \end{cases} \quad (4-6)$$

In Eq. 4-2-1,  $G_{choke}$  is the choking mass flux, and it is an unknown value together with  $P_{Fi}(P_1)$ . Therefore, one more equation is necessary to solve system of equations. The momentum equation for fluid flow, which relate the fluid velocity and pressure as shown in Eq. 5, can be applied.

$$\frac{\partial \rho u_i}{\partial t} + \frac{\partial(\rho u_i u_j)}{\partial z_j} = -\frac{\partial P}{\partial z_i} + \frac{\partial \tau_{ij}}{\partial z_j} + \rho g_i \quad (5)$$

If integrating Eq. 5 at a given control volume and applying Gauss theorem by neglecting the gravitational force, Eq. 5-1 can be obtained.

$$\frac{\partial}{\partial t} \int_{\Omega} \rho u_i dV + \int_{\partial\Omega} \rho u_i u_j dA = - \int_{\partial\Omega} \rho n_i dA + P \int_{\partial\Omega} n_i dA + \int_{\partial\Omega} \tau_w \delta dA \quad (5-1)$$

Then the pressure distribution, Eq. 5-2, along the control volume can be obtained by assuming steady state and 1-D model. The friction coefficient  $f$  is calculated by the Blasius profile based correlation for fully developed turbulent flow.

$$P_{j+1} = \frac{1}{2}P_j \left( \frac{A_j}{A_{j+\frac{1}{2}}} + \frac{A_{j+1}}{A_{j+\frac{1}{2}}} \right) - \rho_{j+1}u_{j+1}^2 \frac{A_{j+1}}{A_{j+\frac{1}{2}}} + \rho_j u_j^2 \frac{A_j}{A_{j+\frac{1}{2}}} - \frac{f \rho_{j+\frac{1}{2}} u_{j+\frac{1}{2}}^2 \pi}{A_{j+\frac{1}{2}}} (D_j \Delta z_j + \frac{1}{2} \Delta D_j \Delta z_j) \quad (5-2)$$

At last, the mass conservation is used for the mass flow rate calculation.

$$G_{Fi} = G_{choke} = \dot{m}_{choke}/A_{Fi} = \rho_j u_j = \rho_{j+1} u_{j+1} \quad (6)$$

### Stage (1→2)

With the value of pressure and mass flow rate at flashing inception point (state1), the two-phase mixture (state2) properties can be calculated by 1-D evaporation wave jump equations. Since the evaporation wave is a discontinuity process, the Rayleigh equation and the Rankine-Hugoniot equation are yielded by combing conservations of mass, momentum, and energy for a control volume enveloping the evaporation front.

Rayleigh equation can be yielded by combing conservations of mass and momentum.

$$G_2^2 = - \frac{(P_2 - P_1)}{(v_2 - v_1)} \quad (7)$$

where

$$G_2 = \frac{\dot{m}_{choke}}{2\pi R_2^2} \quad (7-1)$$

Simoes-Moreira (2002) approximated the cone of evaporation wave as a hemisphere and defined its equivalent radius as

$$R_2 = \sqrt{\dot{m}_{choke} v_2 / 2\pi u_2} \quad (7-2)$$

For a choking condition at a given upstream state, refrigerant velocity at downstream of evaporation wave is sonic, which yield Chapman-Jouguet point. Simoes-Moreira (2003) proved that the Chapman-Jouguet point is a condition of maximum superficial mass flow rate, whose mathematical statement is given by  $dG^2 = 0$ . Therefore, Eq. 8 is obtained through applying the condition of maximum to Rayleigh equation.

$$\frac{dv_2}{dT_2} = - \frac{1}{G_2^2} \frac{dP_2}{dT_2} \quad (8)$$

Meanwhile, the Rankine-Hugoniot equation can be yielded by combing conservations of mass, momentum and energy.

$$(h_2 - h_1) = \frac{v_1 + v_2}{2} (P_2 - P_1) \quad (9)$$

The downstream specific volume is given by mixing rule using void fraction  $v_2 = (1 - \alpha_2)v_{L2} + \alpha_2 v_{V2}$ . Since the downstream two-phase mixture is homogeneous and in thermal equilibrium, one can obtain the downstream void fraction by combining Rankine-Hugoniot equation, resulting in

$$\alpha_2 = \frac{2(h_1 - h_{L2}) + (v_{L2} + v_1)(P_2 - P_1)}{2(h_{V2} - h_{L2}) - (v_{V2} - v_{L2})(P_2 - P_1)} \quad (10)$$

At last, Zivi (1964) or Premoli's (1971) void fraction model can be used to calculate value of downstream vapor quality.

$$x_2 = \frac{1}{1 + \frac{1 - \alpha_2 \rho_L}{\alpha_2 \rho_V} S} \quad (11)$$

Eqs. (8) and (11) along with an saturated thermodynamic property, form a system of non-linear equations that can be solved by iteration method to obtain the downstream pressure  $P_2$  for the given upstream flashing inception point.

### Stage (2/3→4)

From the downstream of evaporation wave, the sonic refrigerant flow undergoes a shock wave accompanied with an abrupt pressure rise to match the EEV exit pressure. Wang et al. (2010) first presented a thorough review of pressure recovery model for two-phase flow across sudden expansion, and explained how the homogeneous pressure recovery model, Eq.12, was obtained from the mass and momentum balances. They also proposed modified homogeneous pressure recovery model by taking account the influence of Bond number, Weber number, Froude number, liquid Reynolds number and vapor quality in to the original homogeneous model.

$$\Delta P_{homogeneous} = G_2^2 \frac{A_2}{A_4} \left(1 - \frac{A_2}{A_4}\right) \left[ \frac{x_2}{\rho_{V2}} + \frac{(1 - x_2)}{\rho_{L2}} \right] \quad (12)$$

The proposed modified homogeneous model for abrupt pressure rise  $\Delta P_{2-4}$  takes the form as

$$\Delta P_{2-4} = \Delta P_{homogeneous} \times (1 + \Omega_1 - \Omega_2) \times (1 + \Omega_3) \quad (13)$$

where

$$\Omega_1 = \left( \frac{We_2 Bo_2}{Re_{Lo_2}} \right)^2 \times \left( \frac{1 - x_2}{x_2} \right)^{0.3} \times \frac{1}{Fr_2^{0.8}} \quad (13-1)$$

$$\Omega_2 = 0.2 \times \left( \frac{\mu_{V2}}{\mu_{L2}} \right)^{0.4} \quad (13-2)$$

$$\Omega_3 = 0.4 \times \left( \frac{x_2}{1 - x_2} \right)^{0.3} + 0.3 \times e^{\frac{1.6}{Re_{Lo_2}^{0.1}}} - 0.4 \times \left( \frac{\rho_{L2}}{\rho_{V2}} \right)^{0.2} \quad (13-3)$$

Here, the Bond number ( $Bo = \Delta \rho g D^2 / \sigma$ ) represents the balance of buoyancy force and surface tension force, the Weber number ( $We = G^2 D / \sigma \rho_h$ ) is the ratio between the mixture inertia and liquid surface tension, the Froude number ( $Fr = G^2 / \rho_h^2 g D$ ) is the ratio between the mixture inertia and the buoyancy force. Meanwhile, the liquid Reynolds number ( $Re_{Lo} = GD / \mu_{L2}$ ) is used as a significant parameter for the two-phase frictional pressure drop correlation.

With the calculated abrupt pressure rise value, the maximal choking occurrence pressure  $P_{oc}$  can be obtained by Eq. 14 as

$$P_{oc} = P_2 + \Delta P_{2-4} \quad (14)$$

## 2.2 Non-choked flow condition

Non-choked flow refers to the condition that the EEV exit pressure is smaller than the maximal choking occurrence pressure  $P_{oc}$ . The non-choked flow can be separated to phase changed flow and non-phase changed

flow depends on whether the EEV exit pressure is smaller than saturation pressure  $P_s$  or not. In both flow conditions, pressure undershoot equation, Eq.4, and momentum equation, Eq.5, can be used to calculate the mass flow rate.

When the refrigerant flow through EEV is phase changed flow ( $P_{oc} < P_{exit} < P_s$ ), the EEV outlet condition is two phase flow. To solve the flashing flow equation systems, the flashing inception point is still assumed to occur at the throat, and a new flashing inception pressure  $P_{Fi,new}$  have to be defined. Since the non-choked mass flow rate increases with EEV exit pressure,  $P_{Fi,new}$  can be defined by relations of  $P_s$ ,  $P_{oc}$ ,  $P_{exit}$  and  $P_{Fi}$ . In this work, a linear change law was applied, and Eq. 15 is derived for  $P_{Fi,new}$  calculation.

$$\frac{P_s - P_{exit}}{P_s - P_{oc}} = \frac{P_s - P_{Fi,new}}{P_s - P_{Fi}} \quad (15)$$

In the same way,  $P_{Fi,new}$  is defined to  $P_{exit}$ , when the refrigerant flow through EEV is non-phase changed flow ( $P_{exit} \geq P_s$ ), because the EEV outlet condition is single phase flow. Then the flashing flow equation systems, including the momentum equation, can be used to calculate the mass flow rate.

According to the discussion above, the EEV mass flow rate modeling methodology for choked flow and non-choked flow is introduced. If numerically solving mathematical equations listed above together with specific refrigerant's properties, one can easily map the mass flow rate at any given inlet conditions and openness of an EEV product.

### 3. MODEL VERIFICATION

As commonly known, EEV's orifice diameter is fixed by manufacture, and the openness can be changed through movement of EEV's needle which is driven by a step motor. Therefore, a special step pulse can yield an effective diameter for corresponding flow area. Meanwhile, the physical shape of EEV's needle determines the flow characteristics of the EEV. Fig. 4 graphically shows the physical shape of EEV's needle which can be classified into liner, equal percentage and quick opening type.

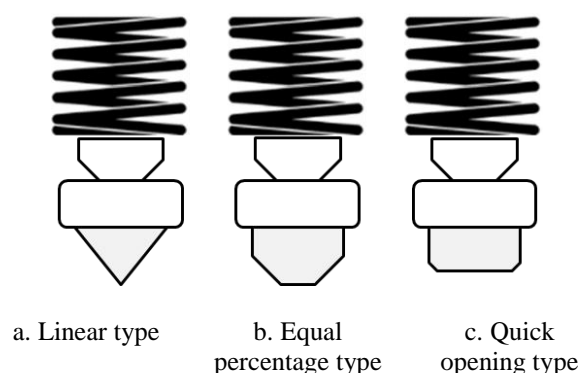


**Figure 4:** Physical shape of EEV's needle

In this work, a quick opening type of EEV needle is used to verify the proposed modeling methodology. Fig.5. shows graphical representation of effective throat area ( $A_{th}$ ) for the refrigerant's flow path. In fact, the throat effective area is side surface area of the frustum of a cone, which can be calculate from shortest distance between needle and orifice ( $L$ ) at corresponding EEV openness together with orifice diameter ( $D_{orifice}$ ) and angle of needle ( $\theta$ ). Here, the needle and orifice distance is the most critical one, and scanning electron microscope (SEM) is used to measure the value under different EEV openness. Then, the effective throat area is acquired, and it is converted to effective throat radius, as Eq.16 shows, for the convenient use in the model.

$$R_{throat} = 0.00034463 * \ln(EEV_{pulse}) - 0.00143117 \quad (16)$$

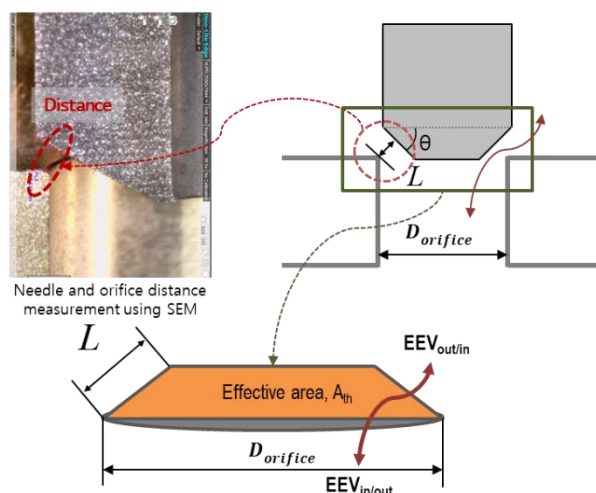


**Figure 5:** Graphical representation of effective throat area for refrigerant's flow path

The model verification condition, which includes EEV inlet pressure and temperature, EEV outlet pressure and EEV openness, is from laboratory tested data. A R410A variable refrigerant flow (VRF) air-conditioning system is operated under cooling condition for the generation of above data. The VRF system consists of 1 outdoor unit and 6 indoor units, and pressure sensors and mass flow rate meter is installed for each indoor units. Fig.6. shows 8553 sets of experimental data from 3 different indoor units using the same type of EEV. It can be observed that system operating condition varies in a certain range, which is good for the model verification under different conditions.

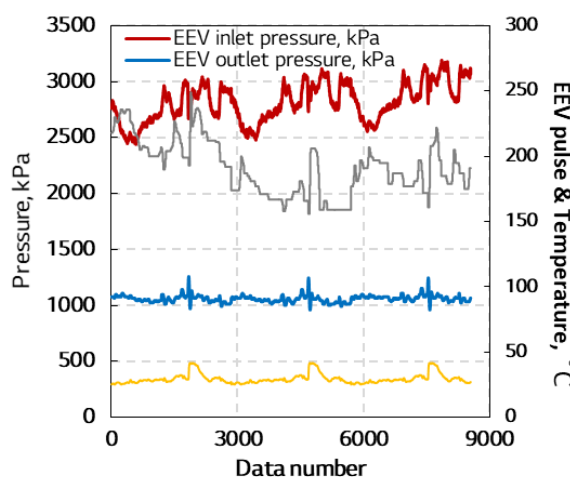


**Figure 6:** Experimental data for EEV model verification

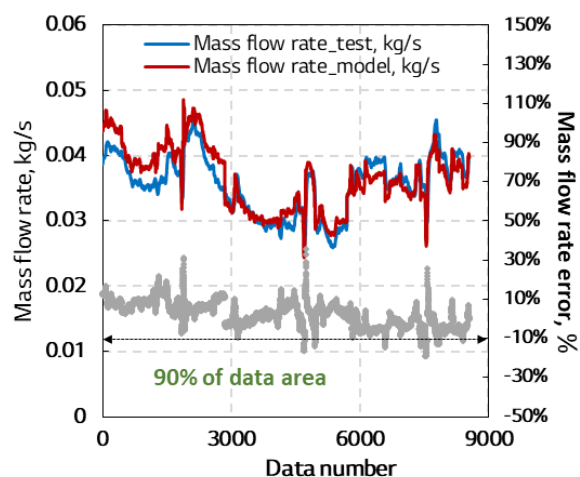


**Figure 7:** Verification result of EEV model

As a result of the verification, it can be observed from Fig.7 that the trend of refrigerant flow change is well simulated. Quantitatively, 90% of the results were accurate within  $\pm 10\%$ , and the left results with lower accuracy happen at the moment of sudden change of mass flow rate due to instable refrigeration cycle conditions.

#### 4. CONCLUSION

This work investigates geometry based EEV's modeling methodology by considering refrigerant's choked flow phenomenon. Theories of the flashing inception and the evaporation wave through nozzles are involved in this methodology. Moreover, the momentum equation is creatively applied to metastable refrigerant flow and numerically calculated with finite volume method both for choked and non-choked flow conditions. The developed modeling methodology is verified with laboratory based EEV's field performance data for R410A, which shows the accuracy for 90% of test data is within  $\pm 10\%$ . At last, it can be concluded that, with proposed methodology, the EEV mass flow rate map for the whole EEV's engineering operation range can be easily generated for different types of EEV products and refrigerant.

## NOMENCLATURE

A	flow area	(m <sup>2</sup> )
Bo	Bond number	(-)
C <sub>m</sub>	mass flow rate coefficient	(-)
D	diameter	(m)
f	friction coefficient	(-)
Fi	inverse of cavitation index	(-)
Fr	Froude number	(-)
g	gravitational constant	(m/s <sup>2</sup> )
G	mass flux	(kg/m <sup>2</sup> /s)
h	enthalpy	(kJ/kg)
k	Boltzmann constant	(-)
$\dot{m}$	mass flow rate	(kg/s)
P	pressure	(Pa)
$\Delta P$	pressure difference	(Pa)
R	radius	(m)
$Re_{Lo}$	liquid Reynolds number	(-)
S	slip ratio	(-)
SEM	Scanning electron microscope	(-)
t	time	(s)
T	temperature	(°C)
T <sub>c</sub>	critical temperature	(K)
TR	reduced temperature	(K)
u	velocity	(m/s)
$\frac{\sqrt{u_i^2}}{u}$	turbulent intensity	(-)
We	Weber number	(-)
x	quality	(-)
Y	expansion factor	(-)
z	distance	(m)
<b>Greek letters</b>		
$\alpha$	void fraction	(-)
$\mu$	viscosity	(Ns/m <sup>2</sup> )
$\rho$	density	(kg/m <sup>3</sup> )
$\Delta\rho$	density difference of liquid&gas	(kg/m <sup>3</sup> )
$\sigma$	surface intension	(N/m)
$\nu$	specific volume	(m <sup>3</sup> /kg)
$\Sigma$	depressurization rate	(millionATM/s)
$\Omega$	correlation factors	
<b>Subscripts</b>		
0	EEV inlet condition	
1	downstream of metastable liquid	
2	downstream of evaporation wave	
3	downstream of shock wave	
4	EEV outlet condition	
cond	condensing	
eev	electronic expansion valve	
eff	effective	
eva	evaporating	
in	inlet	
L	liquid state	
V	vapor state	
oc	occurrence of choked flow	
s	saturated	

## REFERENCE

- Abuaf, N., Jr. Jones, O.C., Wu, B.J.C. (1983). Critical flashing flows in nozzles with subcooled inlet conditions, *ASME J. Heat Transfer*, 105, 379–383
- Alamgir, M. D., Lienhard, J. H. (1981). Correlation of Pressure Undershoot During Hot Water Depressurization, *ASME J. Heat Transfer*, 103, 52-55
- Cao, X., Li, Z.Y., Shao, L.L., Zhang, C.L. (2016). Refrigerant flows through electronic expansion valve: Experiment and neural network modeling, *Appl. Therm. Eng.*, 92, 210-218
- Chen, L., Liu, J. H., Chen, J.P., Chen, Z. J. (2009). A new model of mass flow characteristics in electronic expansion valves considering metastability, *Int J Therm Sci.*, 48, 1235-1242
- Davies, A. Daniels, T.C. (1973). Single and two-phase flow of dichlorodifluoromethane, R12 through sharp-edged orifices, *ASHRAE Trans.*, 79 (Part 1), 109-123
- Fior Markets, (2020). Global Electronic Expansion Valves (EEVs) Market 2020 by Manufacturers, Regions, Type and Application, Forecast to 2025, Part of SUMMARY
- Jr. Jones, O. C. (1980). Flashing Inception in Flowing Liquids, *J. Heat Transfer*, 102(3), 439-444
- Knabben, F.T., Melo, C., Hermes, C.J.L. (2020). A study of flow characteristics of electronic expansion valves for household refrigeration applications, *Int. J. Refrig.*, 113, 1–9
- Li, W.H. (2013). Simplified modeling analysis of mass flow characteristics in electronic expansion valve. *Appl. Therm. Eng.*, 53, 8–12
- Liu, J.H., Chen, J.P., Chen, Z.J. (2008). Investigation on the choking flow characteristics in electronic expansion valves, *Int J Therm Sci.*, 47 (5), 648-658
- Park, C., Cho, H., Lee, Y., Kim, Y. (2007). Mass flow characteristics and empirical modeling of R22 and R410A flowing through electronic expansion valves, *Int. J. Refrig.*, 30 (8), 1401-1407
- Premoli, A., Francesco, D., Prina, A. (1971). A dimensionless correlation for determining the density of two-phase mixtures, *Ric. termotec.*, 25, 17-26
- Roming, R.P., Rothfus, R.R., Kermod, R.I. (1966). Partial vaporization in orifices and valves, *Ind. Eng. Chem. Process. Des. Dev.*, 5, 73-78
- Simoes-Moreira, J.R. (2000). Oblique evaporation waves, *ShockWaves*, 10, 229–234
- Simoes-Moreira, J.R., Vieira, M.M., Angelo, E. (2002). Highly expanded flashing liquid jets, *J Thermophys Heat Trans.*, 16 (3), 415–424
- Simoes-Moreira, J.R., Bullard, C.W. (2003). Pressure drop and flashing mechanisms in refrigerant expansion devices, *Int. J. Refrig.*, 26 (7), 840-848
- Tian, Z., Gu, B., Qian, C., Yang, L., Liu, F. (2015). Electronic expansion valve mass flow rate prediction based on dimensionless correlation and ANN model, *Int. J. Refrig.*, 57, 1-10
- Wan, H.L., Cao, T., Hwang, Y.H., Oh, S.K. (2019) An electronic expansion valve modeling framework development using artificial neural network: a case study on VRF systems, *Int. J. Refrig.*, 107, 114-127
- Wang, C.C., Tseng, C.Y., Chen, I.Y. (2010). A new correlation and the review of two-phase flow pressure change across sudden expansion in small channels, *Int. J. Heat Mass Transf.*, 53 (19), 4287-4295
- Wile, D.D. (1935). The measurement of expansion valve capacity, *Refriger. Eng.*, 8, 108-112
- Xue, Z.F., Shi, L., Ou, H.F. (2008). Refrigerant flow characteristics of electronic expansion valve based on thermodynamic analysis and experiment, *Appl. Therm. Eng.*, 28, 238–243
- Zhang, C., Ma, S.W. Chen, J.P., Chen, Z.J. (2006). Experimental analysis of R22 and R407c flow through electronic expansion valve, *Energy Convers. Manag.*, 47 (5), 529-544
- Zivi, S. M. (1964). Estimation of steady-state steam void-fraction by means of the principle of minimum entropy production, *J. Heat Transf.*, 86(2) 247-251